Ryszard S. Choraś[1]
ORCID: 0000-0002-1706-1219

Bydgoszcz University of Science and Technology
Department of Telecommunications
Computer Sciences and Electrical Engineering
al. prof. S. Kaliskiego 7, 85-796 Bydgoszcz, Poland

[1] choras@pbs.edu.pl

Forearm vein pattern recognition using features from visible and NIR images

DOI: 10.34739/si.2024.30.01

Abstract. Forearm vein recognition is one of many available methods used for identification. However, forearm veins can be considered more secure compared to other biometric traits because the veins are inside the human body and therefore not easily manipulated. Veins possess several properties that make a good biometric feature for personal identification: 1) they are difficult to damage and modify; 2) they are difficult to simulate using a fake template; and 3) vein information can represent the liveness of person. Features were extracted from each pair of visible and NIR images. For the visible images, feature extraction was done using the Gabor filter. For the NIR forearm images, a crossing number was used to extract properties of the veins e.g. bifurcation. We present the results of the recognition of forearm veins patterns that show the suitability of the method for biometric identification purposes.

Keywords: biometrics; vein patterns; feature extraction; Gabor filters; classification

1 Introduction

Images play an important role in the identification of people across many applications. Effective biometrics systems have five key modules: A Sensor or sensors (for image/data acquisition), a Feature Extractor, a Biometric Database, a Matcher and a Decision-Maker. The Sensor reads the biometric information from the user. Feature Extractor module automatically extracts features from the biometric images/templates. All features can be coarsely classified into low-level features and high-level features. Low-level features are extracted directly from the original images, whereas high-level feature extraction must be based on low-level features. The number of features can be reduced before being used in the classification task. Matcher module measures the similarity between extracted features from a user template and an enrolled template. More specifically, the Matcher component of the system compares feature vectors obtained from the feature extraction algorithm to produce a similarity score. This score indicates the degree of similarity between a pair of biometrics data under consideration. The Decision-Maker interprets the result. The Biometric Database maintains the templates of the enrolled users (i.e. the candidate identities).

Biometric categories can be divided into two types: (i) Identification systems and (ii) Verification systems.

Identification systems give an answer to the question: *Who is it?*. In other words, they are performing a one-to-many comparison.
Mathematically, the threshold based identification problem can be formulated as follows: Let $I_1, I_2, ..., I_N$ be the identities of enrolled users; I_{N+1} indicate the reject case; $X_1, X_2, ..., X_N$ be the corresponding biometric templates of the users enrolled.

$$X_Q = \begin{cases} I_k & \text{if } \max\limits_k\{S(X_q, X_I)\} \geq T_S \text{ or} \\ & \min\limits_k\{D(X_q, X_I)\} \leq T_D \\ I_{N+1} & otherwise. \end{cases} \tag{1}$$

where
$S(X_Q, X_k)$ is the similarity measure between X_Q and X_k;
T_S is a predefined threshold for S;
$D(X_Q, X_k)$ is the distance measure between X_Q and X_k; and
T_D is a predefined threshold for D.

Verification systems give an answer to the question: *Is this person who they say they are?* (one-to-one comparison).
Verification can be formulated mathematically as:

$$(I, X_q) = \begin{cases} W_T \text{ if } S(X_q, X_I) \geq T_S \text{ or } D(X_q, X_I) \leq T_D \\ W_F \qquad\qquad otherwise. \end{cases} \tag{2}$$

where
X_q is an input feature vector;
X_I is the biometric feature template belonging to user I from the database;

$S(X_q, X_I)$ is the similarity measure between X_q and X_I;
T_S is a predefined threshold for S;
$D(X_q, X_I)$ is the distance measure between X_q and X_I; and
T_D is a predefined threshold for D.

Desired biometric characteristics are presented in Table 1.

Table 1. Biometrics characteristics

Characteristic	Description
Robustness	Describes by the probability that a submitted template will not match the enrollment the image. Measured by the "false non-match rate".
Distinctiveness	Show how well the biometric separates one individual from another. Measured by the "false match rate".
Permanence	Display how well the biometric remains the same over time. The characteristic is not changing in time.
Acceptability	Describes by polling the device users
Accessibility	Indices by the number of individuals that can be processed in a unit time
Availability	Describes by the probability that a user will not be able to supply a readable measure to the system upon enrollment
Universality	Show how commonly the biometric is found in humans
Performance	Demonstrate the accuracy of the system using the biometric
Circumvention	Indices how easily a submitted template can be spoofed
Uniqueness	No two individuals possess the same characteristic.

Vein recognition is a method of biometric identification/verification, that uses pattern recognition techniques based on images of blood vessels. Blood vessel patterns (identified only on a live body) are unique to each individual. Vein recognition does not require contact during registering and authentication and is strongly immune to forgery [25].

To detect forearm veins and generate a vasculature map we utilize a camera containing two Charge-Coupled Devices (CCD) with two spectral filters - one is a visible light filter and the other is an IR filter. Example visible and NIR forearm images shown in Figure 1.

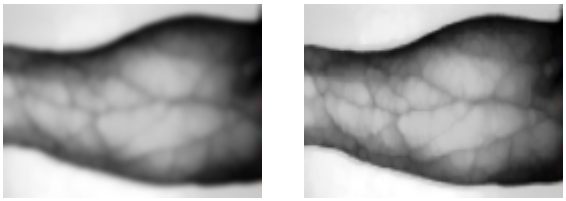

a) b)

Figure 1. Example visible and NIR forearm images

Existing vein recognition methods can be roughly divided into two categories. The first category are methods that determine feature points within the images and match through the

spatial relationships among feature points. The other category of methods combine the global features of two vein images. The human forearm vein recognition presented in this article describes a system based on visible and NIR images that uses geometric and spectral features. The structure of the paper is as follows. In Section 2, information about vein image preprocessing is provided. In Section 3, the proposed method for feature extraction is presented. Then in Section 4, experimental results are provided, which are followed by conclusions and suggestions for future work in Section 5.

1.1 Related Works

Most related published work uses vein templates for the biometrics person recognition process. Classic approaches are presented in Table 2.

Table 2. Summary of work on the vein biometric recognition

Biometric template	Methods	Image	References
Hand vein	• FFT based phase correlation	NIR	[22,25]
	• Distance between feature points	NIR	[4,27]
	• Matching vein triangulation and shape features	NIR	[11]
Finger vein	• Local Binary Pattern (LBP) method using a support vector machine (SVM)	NIR	[12,25]
	• Normalized cross-correlation	NIR	[9]
	• Radon transform	NIR	[23]
	• Local derivative pattern	NIR	[13]
	• Multiscale, curvelets	NIR	[32,8]
Dorsal hand vein	• Curvelet transform	NIR	[32,14]
	• LPP (Locality Preserving Projections)	NIR	[**?**]
	• Shearlet transformation and Scale-invariant Feature Transformation (SIFT)	NIR	[29,15]
Palm vein	• Local Binary Patterns (LBPs) and their variants	NIR	[24,18]
Retina vein	• Local Binary Patterns	Visible	[17]
	• Spectral	Visible	[14,15,17,19]
Ocular vein	• Texture analysis and Statistical parameters	Visible	[21,28,6,19,26]
Forearm vein	• Line Edge Map (LEM)	NIR, Visible	[8]
	• 2D-Gabor + feature extraction	NIR, Visible	[30,2,3]
	• Skeletonization	NIR, Visible	[7,2,3]
	• Shape features	NIR, Visible	[11]

We propose a novel method for personal recognition, extracting features from images in both the visible light and NIR spectrums. Based on these characteristics recognition can be realized.

2 Vein Image Processing

A gray scale digital image of size $M \times N$, $M = 2^i$, $N = 2^j$, can be mathematically defined as a matrix with entries $f(x, y)$, $x = 0, 1, \ldots, M-1$, $y = 0, 1, \ldots, N-1$, where the value $f(x, y)$ represents the intensity or gray level of the image at the pixel (x, y).

$$f(x,y) = \begin{bmatrix} f(0,0) & f(0,1) & \ldots & f(0,N-1) \\ f(1,0) & f(1,1) & \ldots & f(1,N-1) \\ \vdots & \vdots & \ldots & \vdots \\ f(M-1,0) & f(M-1,1) & \ldots & f(M-1,N-1) \end{bmatrix} \tag{3}$$

where $0 \leq f(m,n) \leq G-1$; $G = 2^k$.

Figure 2 shows an overview of our proposed system. In the processing module, processes such as image stretching, image binarization, noise elimination and thinning are applied to extract a normalized and useful forearm image.

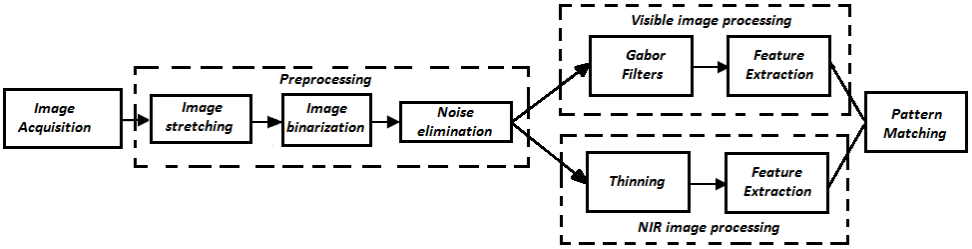

Figure 2. Processing diagram

Each step shown in the processing module Figure 2 will be explained in more detail below [5].

1. Image enhancement. Forearm vein image usually have poor contrast and noise. Contrast enhancement techniques can be used to improve the image [1]. We used CLAHE (Contrast Limited Adaptive Histogram Equalization) [33] for this purpose.
   If h_g represents the number of pixels in an image with intensity g e.g. $f(m,n) = g$, then the probability density function is defined as $prob(f(m,n) = g) = \frac{h_g}{M \cdot N}$ for $g = 0, 1, \ldots, G-1$ and the cumulative density function is defined as $c(f(m,n) = g) = \sum_{g=0}^{G-1} prob(f(m,n)) = g$ for $g = 0, 1, \ldots, G-1$. The gray levels are modified as
   $$\bar{g} = (max - min) \cdot c(f(m,n) = g) + min \tag{4}$$
   where max and min are respectively the maximum and minimum value of image gray level.
   The result after using CLAHE on the images in Figure 1a and Figure 1b are illustrated in Figure 3a and Figure 3b, respectively.

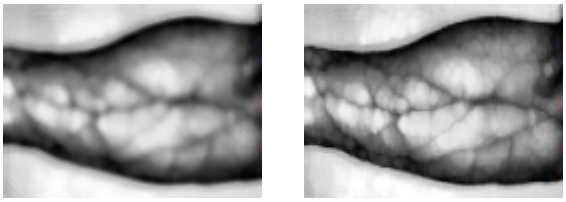

a) b)

Figure 3. The visible and *NIR* forearm images after applying CLAHE

2. Image binarization. Let the initial global threshold (point between two peaks in the histogram) be th. Using th we produce two groups of pixels: the first with all pixels having intensity values $> th$, the second with pixels having values $\leq th$. Next, compute the mean intensity values $mean_1$ and $mean_2$ for the pixels within the first and second groups, respectively. Finally, a new threshold value is defined by $T = \frac{mean_1+mean_2}{2}$.

3. Noise elimination. Median filtering is a nonlinear method based on image statistics used to remove noise. Values in the digital image are assumed to be noisy and replaced by the median value of the neighborhood pixels (the mask).
The pixels belonging to the mask are ranked in the order of their gray levels, and the median value of the group is stored to replace the noisy value.
The 2D MF for an image $f(x, y)$, where $(x, y) \in R$ is defined as

$$p(x, y) = median_{A_l} f(x, y) = median[f(m + r, n + s) \quad ; \quad (r, s) \in A_l] \tag{5}$$

where A_l is the MF window.

3 Texture Feature from Gabor Wavelet Transform

The texture of an image or image segment can be characterized by a set of linear filter responses defined for different spatial frequencies, spatial localization and orientation. The Gabor filter can be written as

$$G_{\sigma_k,\theta_i}(x, y) = \frac{1}{2\pi\sigma_k^2} e^{(-\frac{x^2+y^2}{2\sigma_k^2})} \times \exp\{2\pi j(Wx\cos\theta_i + Wy\sin\theta_i)\} \tag{6}$$

where: $j = \sqrt{-1}$,
σ_k - the standard deviation of the Gaussian envelop,
W - the radial frequency, and
θ_i - the orientation of the Gabor filters.
In our work these parameters are shown in Table 3.

The result of the convolution operation of the input image with the corresponding Gabor filter is an output image calculated as

$$\Psi_{\sigma_k,\theta_i}(x, y) = f(x, y) \otimes G_{\sigma_k,\theta_i}(x, y) \tag{7}$$

Table 3. Gabor filters parameters

Size	σ	W	θ
5×5	2, 4, 8	1	$\frac{\pi i}{6}$ where $i = 1, \ldots, 6$

where $\otimes$ denotes the 2D convolution operation and $f(x, y)$ is the input image.

The images shown in Figure 4 are the result of the convolution operation of the input image with the above defined set of Gabor filters.

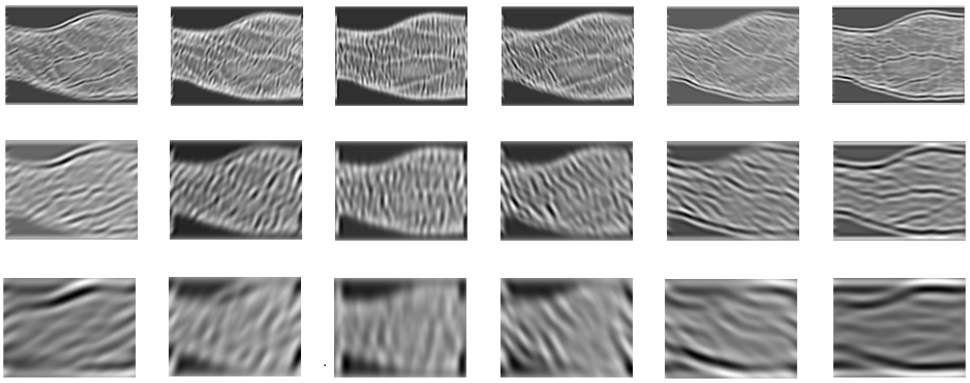

Figure 4. Real part of the Gabor filter responses of a forearm image. Rows correspond to $\sigma_k = \{2, 4, 8\}$, and columns to $\theta_i = \{30°, 60°, 90°, 120°, 150°, 180°\}$.

For each image in Figure 4 we calculate two parameters - energy and entropy (Figure 5) - respectively defined by

$$E_{\sigma_k,\theta_i}(x, y) = \frac{1}{M \times N} \sum_{x=0}^{M-1} \sum_{y=0}^{N-1} (\Psi_{\sigma_k,\theta_i}(x, y))^2 \tag{8}$$

and

$$Ent_{\sigma_k,\theta_i}(x, y) = -p_{\sigma_k,\theta_i}(x, y) \times \log_2(p_{\sigma_k,\theta_i}(x, y)) \tag{9}$$

where

$$p_{\sigma_k,\theta_i}(x, y) = \frac{E_{\sigma_k,\theta_i}(x, y)}{\sum_{\sigma_k} \sum_{\theta_i} E_{\sigma_k,\theta_i}(x, y)} \tag{10}$$

In our case, the feature vector has the size $3 \times 6 \times 2 = 36$ (three scales, six orientations, two parameters) and takes the following form

$$\begin{aligned} FV_1 = \{&E_{2,30}, \ldots, E_{2,180}, E_{4,30}, \ldots, E_{4,180}, E_{8,30}, \ldots, E_{8,180}, \\ &Ent_{2,30}, \ldots, E_{2,180}, Ent_{4,30}, \ldots, E_{4,180}, Ent_{8,30}, \ldots, Ent_{8,180}\} \end{aligned} \tag{11}$$

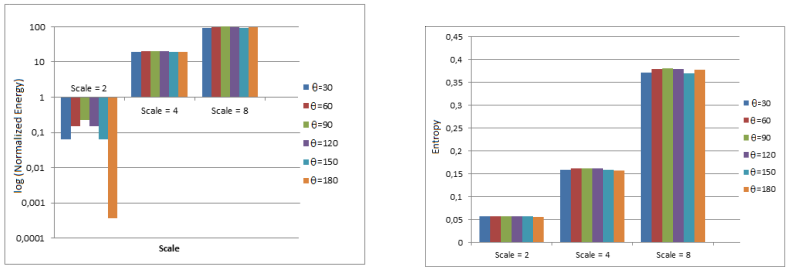

a) b)

Figure 5. Energy and Entropy plots of the Gabor images

4 Extraction of Geometrical Features

The thinning algorithm determines skeletal pixels by local operations. The neighbors around pixel p are enumerated as $p_1, p_2, \ldots, p_8$ (Figure 6). The quantity of such pixels that equal 1, that is $p_i = 1$, $i = 1, 2, \ldots, 8$ pixels is $B(p)$. The number of transitions from 0 to 1 in neighbors around pixel p is $A(p)$ [31].

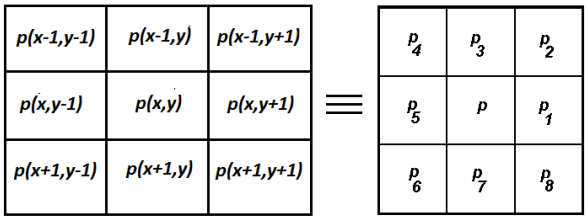

Figure 6. Pixel notations

The point p is deleted from the image if:

(i) $2 < B(p) \leq 6$
(v) $p_3 \cdot p_1 \cdot p_7 = 0$
(u) $p_1 \cdot p_7 \cdot p_5 = 0$

If any condition is not satisfied conditions (v) and (u) are changed to

(iv) $p_3 \cdot p_5 \cdot p_7 = 0$
(iu) $p_1 \cdot p_3 \cdot p_5 = 0$

The results of the vessel preprocessing are shown in Fig. 1.

The Crossing Number (CN) concept [10,16] is used to specify bifurcations points in the skeleton vessels image. The Crossing Number CN at a point p with a neighborhood of points p_i is obtained according to the formula:

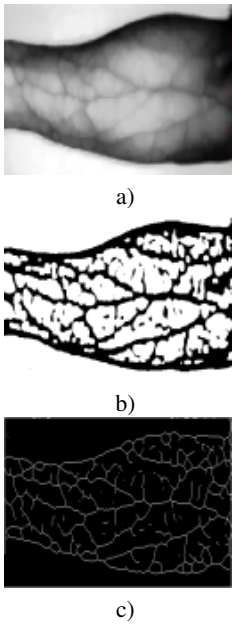

a)

b)

c)

Figure 7. (a) The original forearm vein image; (b) the result of binarization; and (c) the skeleton of the vein region

$$CN = \frac{1}{2}\sum_{i=1}^{8} |p_i - p_{i+1}|, \quad p_9 = p_1 \tag{12}$$

Properties of the point p are shown in Table 1.

Table 4. Topological properties of p

THE VALUE OF CN	PROPERTY OF PIXEL p
0	Internal or isolate
1	end
2	connect
3	bifurcation
4	cross

The vessel topology is described by the feature vector FV_2 which defines bifurcation structure:

$$\begin{aligned} FV_2 &= \{position\ of\ bifurcation\ points,\ angles\} = \\ &= \{bif_1, bif_2, \ldots, bif_h\} \end{aligned} \tag{13}$$

where
h - the number of bifurcation points in the forearm image,
$bif_h = \{x_h, y_h, \alpha_{1h}, \alpha_{2h}, \alpha_{3h}\}$. (x_h, y_h) are position of bifurcation points and $(\alpha_{1h}, \alpha_{2h}, \alpha_{3h})$ are the bifurcation angles with respect to the horizontal axis.

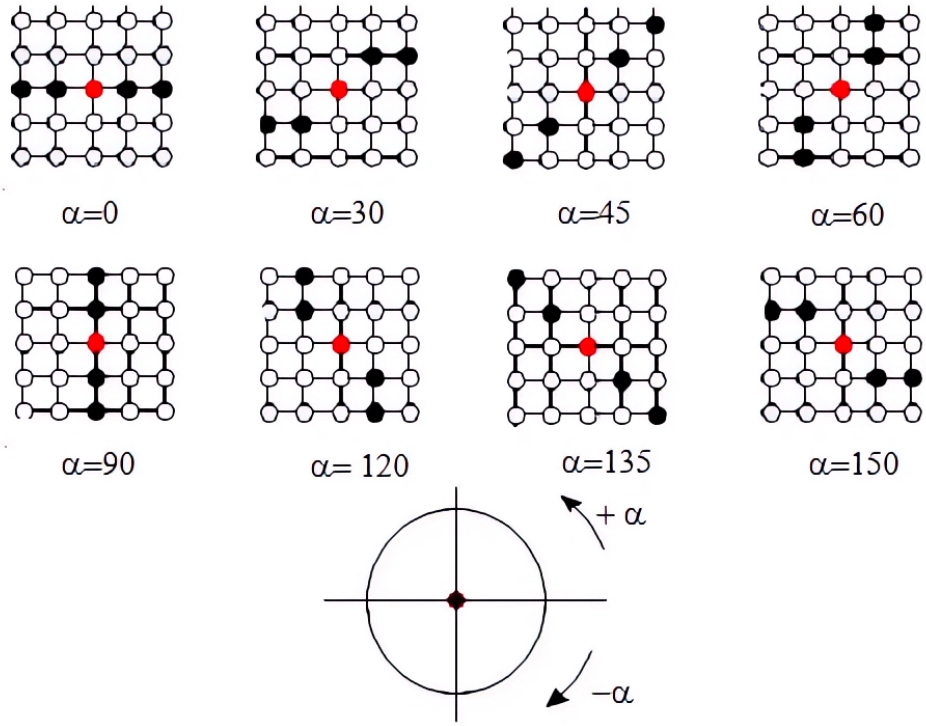

Figure 8. Possible directions of orientation of bifurcation points

The normalized image of size (128×96) pixels is divided into non-overlapping blocks of (32×32) pixels. In this way we obtain 12 blocks numbered from left to right and from top to bottom.

70 bifurcation points have been detected in Figure 9 and these points assigned to individual blocks are presented in Table 5. Possible orientations of bifurcation points randomly selected from Table 5 are shown in Figure 10.

As a results of the anatomical topology of the blood vessels of the forearm, and confirmed by the data contained in Table 5, the most characteristic points are found in blocks 5,6,7,8. In these blocks we limit the number of bifurcation points to 10, in blocks 2,3,4, the number of bifurcation points is limited to 5 and in the remaining blocks, we consider only a single

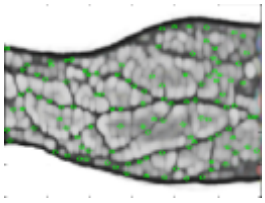

a)

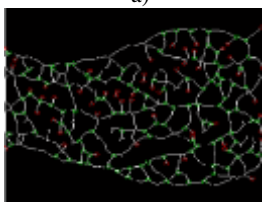

b)

Figure 9. Feature points extracted from forearm images: a) characteristics points on original image; b) bifurcation points on skeleton image

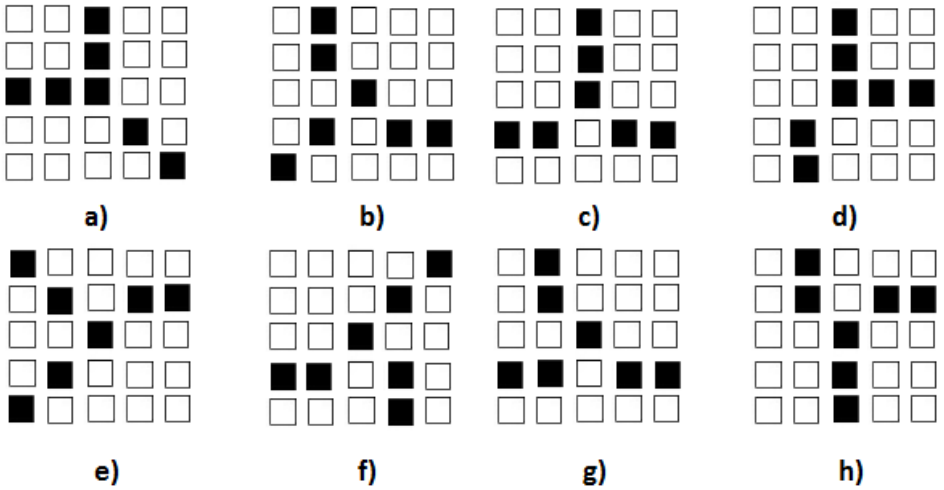

Figure 10. Examples of orientations of the bifurcation points - $(\alpha_1, \alpha_2, \alpha_3)$: a) $(180°, 90°, -45°)$, b) $(-135°, 120°, -30°)$, c) $(150°, 90°, -30°)$, d) $(-120°, 90°, 0°)$, e) $(135°, -135°, 30°)$, f) $(150°, -60°, 45°)$, g) $(-150°, 120°, -30°)$.

bifurcation point.

The selection of bifurcation points in individual blocks is carried out as follows:

Table 5. Feature Vector FV_2 for the image shown in Figure 9

x	y	α_1	α_2	α_3	x	y	α_1	α_2	α_3	x	y	α_1	α_2	α_3	x	y	α_1	α_2	α_3
1					2					3					4				
26	28	135	-90	0	47	32	120	-120	-30	72	32	-150	120	-30	107	31	180	45	-45
					38	30	-150	90	-45	93	29	180	90	-60	103	29	180	30	-45
					39	25	120	-120	0	79	22	180	-60	30	112	25	180	90	-30
					42	23	135	-90	0	71	20	-150	45	-45	111	16	150	60	-60
					54	23	120	-90	0	67	17	180	-60	45	104	14	-135	90	-30
					52	19	180	90	-45	86	14	-135	120	0					
					62	16	150	-90	30	90	13	180	-60	45					
5					6					7					8				
15	34	180	90	-60	41	63	135	45	-45	80	59	-120	90	0	105	62	-150	90	-45
29	44	150	-60	30	47	61	180	60	-30	79	56	-135	60	-45	108	60	120	-120	0
9	44	-150	60	-45	57	61	180	-60	45	65	55	135	-120	0	114	58	135	-120	-30
5	44	135	-90	0	43	61	135	-120	0	80	49	-150	90	-45	106	58	150	-60	45
12	41	-135	120	-30	50	59	150	-90	30	76	48	135	-135	0	109	51	120	-90	30
9	63	-150	45	-45	62	58	180	45	-45	91	47	150	-90	30	111	44	150	-90	0
12	53	-135	90	-30	46	51	120	-120	-30	84	47	180	-120	30	102	38	120	-90	0
23	48	180	60	-45	49	51	180	90	-30	70	46	-150	120	-30					
32	34	120	-60	45	54	44	-135	120	0	75	39	-135	90	0					
					59	44	180	90	-30	79	38	180	-60	45					
					47	41	150	-90	0	90	36	-135	60	0					
					59	35	150	-90	30	70	34	150	45	-45					
					44	34	180	90	-60										
9					10					11					12				
12	66	135	-135	30	59	66	135	-90	30	83	72	180	90	-45	105	74	135	-90	45
20	66	120	-120	-30						94	71	-150	90	-30	104	69	180	60	-45

- the coordinates (x, y) of the bifurcation point are transformed to the local coordinates of the given block $(x_{block_l}, y_{block_l})$, $l = 1, \ldots, 12$,
- $\rho = \sqrt{x^2_{block_l} + y^2_{block_l}}$ is calculated ,
- ρ-values are ranked from the smallest to the largest ,
- as points of the FV_2 vector, the first t points are selected, where t is the number of points specified for the given block.

As a result, we obtain 60 bifurcation points.

5 Pattern Matching

We defined the vectors of features as follows:

$$FeatVec = (FV_1, FV_2) \tag{14}$$

where
FV_1 is the Gabor feature vector, and

FV_2 is the bifurcation feature vector.

The $FeatVec$ feature vector contains 36 + 300 = 336 elements.

The Euclidean distance is the basis for pattern matching between the two vectors associated with Gabor features (FV_1). One vector refers to the input forearm image, the second to the template forearm image. A Euclidean distance less than a certain threshold, allows the conclusion that the input image and the template image are "very similar" or even the same.

In the case of the FV_2 vector, two bifurcation points bif_u and bif_v are considered to match, if their position and orientation are close [20]:

$$D(bif_u, bif_v) = \sqrt{(x_u - x_v)^2 + (y_u - y_v)^2} < Th_1 \tag{15}$$

$$A(bif_u, bif_v) = min(|\alpha_{u_1} - \alpha_{v_1}|, |\alpha_{u_2} - \alpha_{v_2}|, |\alpha_{u_3} - \alpha_{v_3}|) < \Theta \tag{16}$$

If S is higher than a threshold value, then the input forearm image is matched with the template forearm image, otherwise it is considered to not be a match. S is defined as follows

$$S = \frac{H_{uv}}{\sqrt{uv}} \tag{17}$$

where the number of matched bifurcation is H_{uv}.

6 Results

The results of our method are summarized in Table 6.

Table 6. Mean and standard deviation Gabor phase iris image

Number of Visible Forearm Images	Number of NIR Forearm Images	Accuracy Classification Rate
100	–	86.9
–	100	88.25
100	100	94.9

7 Conclusions

In this article we propose method to biometric identification based on forearm vein images. The proposed method uses Gabor filtering to producing the feature vector based on energy and entropy parameters. Second feature vector uses bifurcation points in the skeleton vessels image. A comparison with other methods show that our method gives superior results.

References

1. Choras, R.S. Iris Recognition, Computer Recognition Systems 3, AISC 57, 637-644, Springer-Verlag Berlin Heidelberg, 2009.
2. Choras, R.S. Personal identification using forearm vein patterns. 2017 International Conference and Workshop on Bioinspired Intelligence (IWOBI), **2017**, 1-5.
3. Choras, R.S. Biometric personal authentication using images of forearm vein patterns. 2017 International Conference on Signals and Systems (ICSigSys), **2017**, 40-43
4. Ding, Y., Zhuang, D., Wang, K., A study of hand vein recognition method, Proc. IEEE Intl. Conf. Mechatronics & Automation, **2005**, 2106-2110.
5. Gonzales, R.C., Woods, R.E., Digital Image Processing, Pearson Prentice Hall, 2008.
6. Haralick, R., Shanmugam, K., Dinstein, I. Textural features for image classification. IEEE Trans. on Systems, Man, and Cybernetics, **1973**, SMC-3(6), 610-621.
7. Kang, B.J., et al,. Multimodal biometric method based on vein and geometry of a single finger. IET Computer Vision, **2010**, 4.3, 209-217.
8. Kirbas, C., Quek, K. Vessel extraction techniques and algorithm: a survey. Proceedings of the 3rd IEEE Symposium on BioInfomratics and Bioengineering, **2003**.
9. Kono, M., et al,. Near-infrared finger vein patterns for personal identification. Applied Optics, **2002**, 41(35), 7429-7436.
10. Kumar, A. Incorporating cohort information for reliable palmprint authentication. Proceeding of ICVGIP, **2008**, 583-590.
11. Kumar, A., Prathyusha, K. Venkata., Personal Authentication using Hand Vein Triangulation and Knuckle Shape. IEEE Transactions on Image Processing, **2009**.
12. Lee, H.C., et al, Finger vein recognition usin. Journal of Zhejiang University-SCIENCE C, **2010**, 11(7), 514-524.
13. Lee, E.C., et al., New finger biometric method using near infrared imaging. Sensors, **2011**, 11, 2319-2333.
14. Liu, C. J., Wechsler, H. Gabor feature based classification using the enhanced Fisher linear discriminant model for face recognition. IEEE Transactions on Image Processing, **2002**, 11(4), 467- 476.
15. Liu, D. H., Lam, K. M., Shen, L. S. Optimal sampling of Gabor features for face recognition. Pattern Recognition Letters, **2004**, 25(2), 267-276.
16. Maltoni, D., Maio, D., Jain, A.K., Prabhakar, S. Handbook of Fingerprint Recognition, **2003**, Springer.
17. Meng, X., Yin, Y., Yang, G., Xi, X. Retinal Identification Based on an Improved Circular Gabor Filter and Scale Invariant Feature Transform. Sensors, **2013**, 13, 9248-9266.
18. Pierre-Olivier, L., Christophe, R., Bernadette, D. Palm vein verification system based on SIFT matching. Proceedings of Third International Conference ICB, **2009**, 1290-1298.
19. Park, U., Jillela, R., Ross, A., Jain, A. Periocular biometrics in the visible spectrum. IEEE Trans. Inform. Forensics Secur., **2011**, 6(1), 96-106.
20. Ranade, A., Rosenfeld, A. Point pattern matching by relaxation, Pattern Recognition, **1993**, 12(2), 269-275.
21. Ross, A., Nandakumar, K., Jain, A.K. Handbook of Multibiometrics, Springer, 2006.
22. Tanaka, T., Kubo, N. Biometric authentication by hand vein patterns. Proc. SICE Annual Conference, **2004**, 249-253.
23. Wang, D., et al., User identication based on finger-vein patterns for consumer electronics devices. IEEE Transactions on Consumer Electronics, **2010**, 56.2, 799-804
24. Wang, Y., Li, K., Cui, J. Hand-dorsa vein recognition based on partition local binary pattern. IEEE 10th International Conference on Signal Processing (ICSP), **2010**, 1671-1674.

25. Wang, Y., Hu, J., Phillips, D. A fingerprint orientation model based on 2d fourier expansion (FOMFE) and its application to singular-point detection and fingerprint indexing. IEEE Transactions on Pattern Analysis and Machine Intelligence, **2007**, 29(4), 573-585.
26. Woodard, D., Pundlik, S., Lyle, J., Miller, P. Periocular region appearance cues for biometric identification. Computer Vision and Pattern Recognition Workshops (CVPRW), **2010**, 162-169.
27. Yuksel, A., Akarun, L., Sankur, B. Biometric identification through hand vein patterns. International Workshop in Emerging Techniques and Challenges for Hand-Based Biometrics (ETCHB), **2010**, 1-6.
28. Xueyan, L., Shuxu, G., Fengli, G., Ye, L. Vein pattern recognitions by moment invariants. Proceedings of the First International Conference on Bioinformatics and Biomedical Engineering, **2007**, 612-615.
H. Zhang et al, Finger Vein Recognition Based on Gabor Filter, Intelligence Science and Big Data Engineering (Lecture Notes), (2013) pp. 827-834
29. Zeng, Z., Hu, J., Face Recognition Based on Shearlets and Principle Component Analysis. IEEE International Conference on Intelligent Networking and Collaborative Systems, **2013**, 697-701.
30. Zhang, H., et al. Finger Vein Recognition Based on Gabor Filter. Intelligence Science and Big Data Engineering, **2013**, 827-834.
31. Zhang, T., Suen, C. A fast parallel algorithm for thinning digital patterns, Communications of the ACM, **1984**, 27, 236-239.
32. Zhang, Z., et al. Multiscale Feature Extraction of Finger-Vein Patterns Based on Curvelets and Local Interconnection Structure Neural Network. The 18th International Conference on Pattern Recognition, **2006**, 4, 145-148.
33. Zuiderveld, K. Contrast Limited Adaptive Histogram Equalization, **1994**, Academic Press, Cambridge.